doi: 10.18323/2782-4039-2023-3-65-9

Determination of the volume fraction of primary carbides in the microstructure of composite coatings using semantic segmentation

Natalia N. Soboleva*[1,2,3], PhD (Engineering), senior researcher
Aleksandr N. Mushnikov[1,4], PhD (Engineering), researcher
[1]*Institute of Engineering Science of the Ural Branch of RAS, Yekaterinburg (Russia)*
[2]*M.N. Mikheev Institute of Metal Physics of the Ural Branch of RAS, Yekaterinburg (Russia)*

***E-mail: soboleva@imach.uran.ru, natashasoboleva@list.ru**

[3]ORCID: https://orcid.org/0000-0002-7598-2980
[4]ORCID: https://orcid.org/0000-0001-7073-6476

Received 14.06.2023 *Accepted 15.08.2023*

Abstract: In the process of formation of composite coatings, partial dissolution of strengthening particles (most often carbides) in the matrix is possible; therefore, in some cases, the material creation mode is chosen taking into account the volume fraction of primary carbides not dissolved during coating deposition. The methods currently widely used for calculating the volume fraction of carbides in the structure of composite coatings (manual point method and programs implementing classical computer vision methods) have limitations in terms of the possibility of automation. It is expected that performing semantic segmentation using convolutional neural networks will improve both the performance of the process and the accuracy of carbide detection. In the work, multiclass semantic segmentation was carried out including the classification on the image of pores and areas that are not a microstructure. The authors used two neural networks based on DeepLab-v3 trained with different loss functions (IoU Loss and Dice Loss). The initial data were images of various sizes from electron and optical microscopes, with spherical and angular carbides darker and lighter than the matrix, in some cases with pores and areas not related to the microstructure. The paper presents mask images consisting of four classes, created manually and by two trained neural networks. The study shows that the networks recognize pores, areas not related to the microstructure, and perfectly segment spherical carbides in images, regardless of their color relative to the matrix and the presence of pores in the structure. The authors compared the proportion of carbides in the microstructure of coatings determined by two neural networks and a manual point method.

Keywords: composite coatings; carbides; optical microscopy; scanning electron microscopy; semantic segmentation; neural networks.

Acknowledgements: The work was carried out within the state assignment to the Institute of Engineering Science, UB RAS on the topics No. AAAA-A18-118020790147-4 and No. AAAA-A18-118020790148-1 and the Institute of Metal Physics, UB RAS on the topic “Additivity” No. 121102900049-1.

Microscopic images were obtained using the equipment of the “Plastometry” Core Facility Center of the IES UB RAS.

The paper was written on the reports of the participants of the XI International School of Physical Materials Science (SPM-2023), Togliatti, September 11–15, 2023.

For citation: Soboleva N.N., Mushnikov A.N. Determination of the volume fraction of primary carbides in the microstructure of composite coatings using semantic segmentation. *Frontier Materials & Technologies*, 2023, no. 3, pp. 95–102. DOI: 10.18323/2782-4039-2023-3-65-9.

INTRODUCTION

At present, the industry is imposing increasingly strict requirements to strength, wear resistance, durability, and other working properties of machine parts and tools. To solve the problem of improving the tribological properties of products, new wear-resistant materials and coatings, including composite ones, are constantly being developed [1]. One of the most promising coatings for operation under abrasive wear conditions are “carbide – metal matrix” composite materials [2–4].

For the effective composite coating formation, it is necessary that the matrix has a relatively low melting point, and the carbides have a high one [5]. Thus, when creating a material, a wear-resistant filler will be provided in the form of initial primary particles not dissolved in the matrix. However, carbides can partially dissolve in the matrix when creating composite coatings [6–8], thereby reducing their wear resistance [9]. In this regard, in a number of cases, when developing a coating technology for the resulting prototypes, both the composition and effective properties are studied, and the volume of coarse primary strengthening particles in the microstructural material is determined.

Currently, the standardised method for determining the phase volume fraction is the manual point method according to ASTM E 562-02, which is a labour-intensive process. Simplification of the process is possible by using programs implementing classical computer vision methods, such as Siams, Thixomet, ImageJ, JMicroVision, etc. [10; 11]. However, it was shown in [12] that the use of classical computer vision methods has a number of limitations, that make it difficult to automate the process.

The application of neural networks for segmentation of images of composite materials is a possible problem solution. In this case, semantic segmentation, the process of understanding images at the pixel level [13], is performed, which allows dividing images into the areas corresponding to the semantic class in a predetermined list. A neural

network studies the features of the classes using pre-prepared masks – images marked by different colours. Semantic segmentation combines object detection, shape recognition, and classification.

The use of convolutional neural networks makes it possible to significantly improve the semantic segmentation performance [14]. Over the past few years, many semantic segmentation models, based on convolutional neural networks have demonstrated good performance in the image segmentation tasks, such as FCN, SegNet, RefineNet, U-net, PSPNet, and DeepLab [13; 15; 16]. To produce segmentation maps, the DeepLab model implements an architecture based on a convolutional neural network. In addition to conventional convolutions, discharged convolution kernels are used, which allow considering, more spatial information without increasing the number of parameters [17]. A more advanced DeepLab-v3 version is characterised by the improved performance at high segmentation accuracy [18].

In the work [12], WC tungsten carbide particles were segmented in the structure of NiCrBSi coatings using U-net and LinkNet networks. At the same time, the task of one-class segmentation was solved: pixels were identified, which belonged and did not belong to carbides. The authors of the work note that the trained models had a tendency for incorrect classification of pores, related to the class of carbides.

The present work aims to determine the volume fraction of primary carbides in the microstructure of composite materials, using trained neural networks, based on DeepLab-v3 for semantic segmentation. An implementation feature is multiclass segmentation including classification by image of pores and domains that are not a microstructure.

METHODS

The initial data were images of the microstructure of composite coatings based on nickel and iron with coarse primary tungsten, titanium, and chromium carbides, obtained using a Tescan VEGA II XMU scanning electron microscope and the optical system of a Shimadzu HMV-G21DT microhardness tester. The use of two different methods allowed obtaining images with different characteristics: different sizes (768×840 and 640×480 pixels), TIFF/JPG formats, carbides in microphotographs are lighter and darker than the matrix, the presence/absence of areas that are not a microstructure (areas with shooting parameters and a scale bar). Moreover, the images obtained by both methods were characterised by the presence of pores on some of them, as well as the presence of two types of carbides: spherical and angular. The number of original images was 41.

For convenience, all files were converted to the PNG format. The data set was marked manually in MS Paint (obtaining masks – ground truth images), using four colours: dark gray on the mask image – carbides, black – pores, white – the rest of the microstructure, light gray – the area that is not a microstructure.

The implementation of the deeplabv3_resnet101 model from the torchvision library was taken as a neural network. As the base for the deeplabv3_resnet101 model, the ResNet image classification network of the resnet101 version pre-trained on the Imagenet dataset was used. By default, the number of recognisable classes in the DeepLab-v3 network is 21. In the work, the head of the network was re-trained, with the replacement of the number of output layers in the last convolution by 4 – according to the number of identifiable classes. At the network output, a float tensor with the size of (*B, C, H, W*) is obtained, where *B* is the batch size, *C* is the number of classes, *H* is the image height, and *W* is the image width.

To train the network, the authors used the Adam optimizer. According to the results of preliminary tests, from the traditional range of learning rates for Adam from 10^{-4} to 10^{-3}, a learning rate of $3 \cdot 10^{-4}$ was chosen. The batch size was equal to 32. At the same time, 80 training and 20 testing iterations were performed at each training epoch. The number of epochs was 20.

Two networks were created with the same parameters except for the loss function. For one network, the loss function was based on the Jaccard distance metric, known as IoU (Intersection over Union), and for the other, on the Sörensen–Dice metric (Dice) [19].

Five images with different features were selected for the test set. The remaining 36 images were subjected to the following processing. Since it is preferable to train a neural network using images of the same size, a size of 224×224 pixels was chosen, corresponding to the recommended size for the ResNet network, on the basis of which the selected DeepLab-v3 model is built. Fragments of 224×224 pixels were cut out from the original images and masks with a random step from 50 to 65 pixels along each axis. Then the original images were reduced twice, and the procedure was repeated for the reduced images. The division of the obtained 3148 images into training and testing sets was performed randomly with a ratio of 0.8:0.2.

The trained model allows building a mask from a photograph of a microstructure of arbitrary resolution. To do this, the program cuts the original image into fragments of 224×224 pixels. If the size (width or height) of the original image is not a multiple of 224, the last (in horizontal or vertical direction) square may have an intersection with the penultimate one. The network processes each fragment separately, and then the mask of the entire image is assembled in reverse order. The mask obtained as a result of the neural network operation allows calculating the volume fraction of the content of carbides (dark gray pixels) in the microstructure image as a percentage. In this case, areas not related to the microstructure (light gray pixels) are subtracted from the calculation of the total area occupied by the microstructure.

Comparison of the proportion of carbides, in the microstructure, determined using artificial intelligence was carried out, applying a manual point method for determining the volume fraction of phases according to ASTM E 562. To do this, a 100-points grid was applied to the test images (Fig. 1). The volume fraction of carbides was calculated as the ratio of the number of grid points fell on the carbide to the total number of points. In the case of a point hitting the "carbide-matrix" boundary, it was considered as belonging to both phases, so its contribution to the calculation of the proportion of carbides was 0.5.

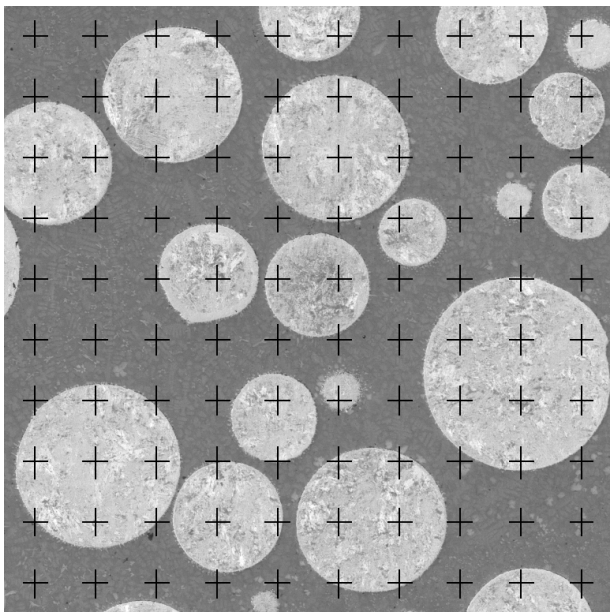

Fig. 1. *An example of determining the fraction of carbides in the microstructure according to ASTM E 562 test method*
Рис. 1. *Пример расчета доли карбидов в микроструктуре по ASTM E 562*

RESULTS

Table 1 shows the microstructure images used as test, as well as image masks using four assigned colours generated by a human (manual marking) and two neural networks trained with different loss functions: IoU Loss and Dice Loss.

It can be observed that the neural networks had no problems when segmenting the areas not occupied by the microstructure (light gray in images 1, 2 and 5). The networks also recognise pores (black in images 4 and 5), and if in image 5 the carbides are lighter than the matrix, and the pore visually differs significantly from them in colour, then in image 4 the carbides are darker than the matrix and, similar to the pore, is spherical. Therefore, adequate pore recognition in this image was not predictable. It can be observed, however, that the network with Dice Loss mistook a small part of the pore for a carbide part.

Artificial intelligence segmentation of carbides, occupying a large volume in images and are characterised by various visual features, was expectedly performed with some errors. Among them is the recognition of carbides in the places of their absence (highlighted by a dashed circle in the image 1 of the network with Dice Loss) and, conversely, the non-recognition of a part of the carbide (highlighted by a dashed circle in images 2, 4, and 5), which was recorded by both networks in the same places. The analysis of this error showed that it is related to cutting the original images into squares of 224×224 pixels, and processing them separately. In this case, a small edge of the carbide appeared in another image, and the network did not recognise it. Probably for the same reason, image 3 is segmented with the largest error, since in some sliced images, large carbide occupied most of the frame.

In general, one can note good recognition of pores by trained neural networks and excellent segmentation in images of spherical carbides, regardless of their colour relative to the matrix and the presence of pores in the structure.

Table 2 calculates the volume fraction of carbides in the microstructure of coatings in test images. It can be observed that the calculation according to ASTM showed good results, compared to the reference calculation according to manual marking, the difference is from 0.5 to 1.3 % of the volume fraction of carbides. The neural network with IoU Loss, showed a difference with the ground truth images from 0.1 to 1.1 %, and the network with Dice Loss – from 0.1 to 0.6 % of carbides. Table 3 shows the mean square error of calculating the fraction of carbides over the entire test set. The calculation by the network with Dice Loss was characterised by the smallest value of the mean square error (0.14), and the calculation according to ASTM – by the largest one (0.80).

However, the mean square error of calculating the fraction of carbides does not fully reflect the quality of the neural network, since it does not consider the "two-sided" errors of the network: finding carbides where they are absent, and not finding where they should be. Therefore, the IoU, Dice, and MeanIoU metrics, the values of which can range from 0 to 1 and tend to 1 in the case of the smallest error in the segmentation of areas, were also defined for neural networks. Despite the less accurate determination of the volume fraction of carbides in percent (Table 2), the network with IoU Loss is characterised by the maximum values of all three metrics (Table 3), which is associated with its smaller inaccuracies (compared to the network with Dice Loss), in the segmentation of the most "problematic" image No. 3 (Table 1).

DISCUSSION

The use of artificial intelligence has a number of disadvantages, in particular, the necessity of collecting and preparing a large amount of data for training a neural network

Table 1. *Microstructure images from test set and imaging of masks created manually and by two neural networks*
Таблица 1. *Изображения микроструктуры из тестового набора и отображение масок, сформированных вручную и двумя нейронными сетями*

No.	Microstructure image	Manual marking	Network with Loss=(1−IoU)	Network with Loss=(1−Dice)
1	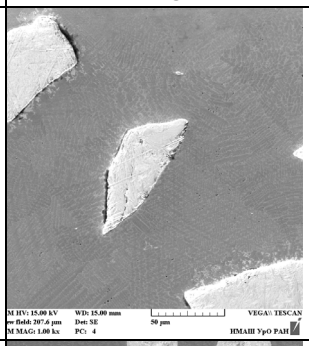	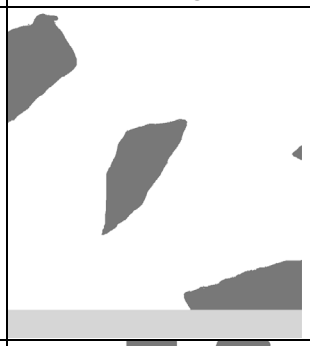	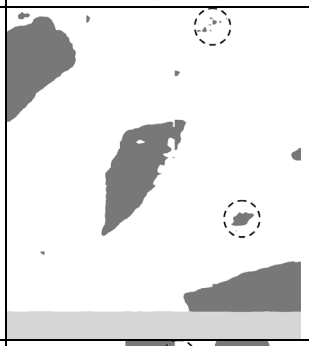	
2	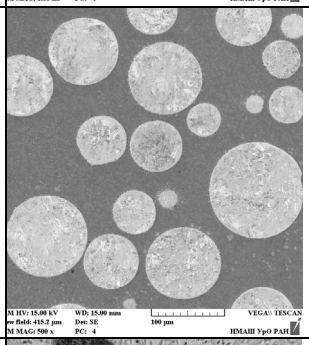	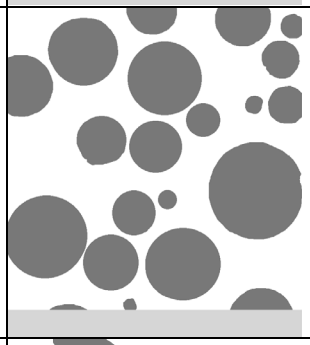	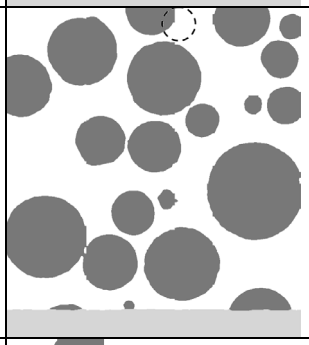	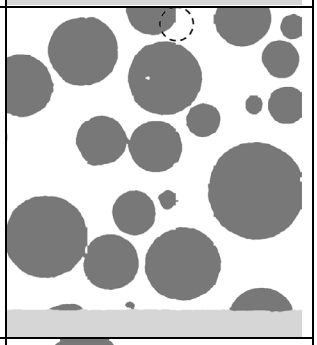
3	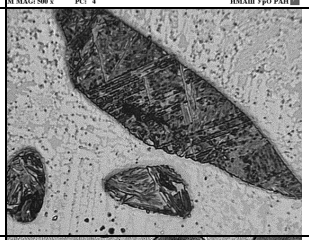	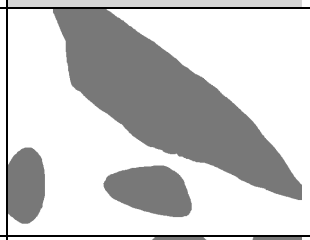	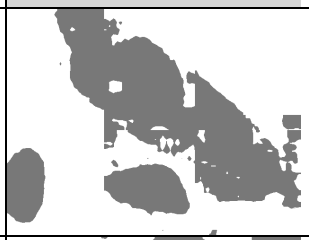	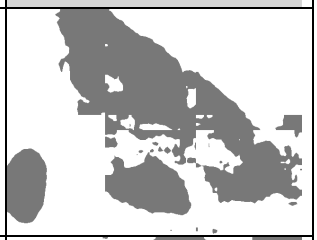
4	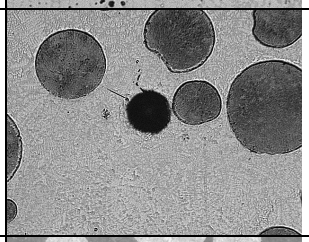	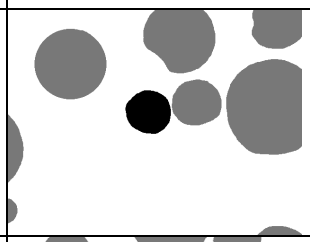	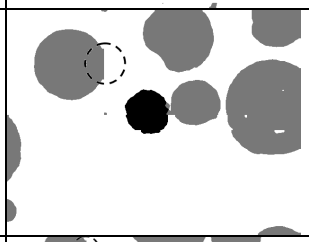	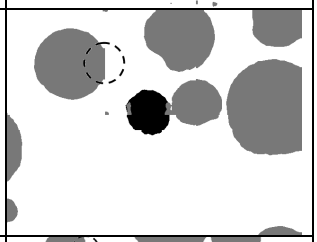
5	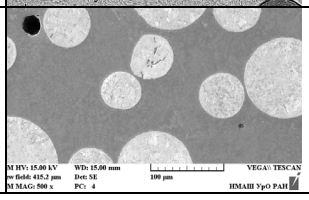	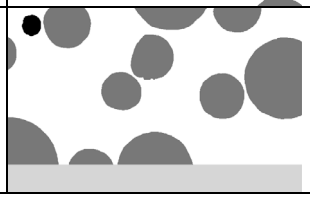	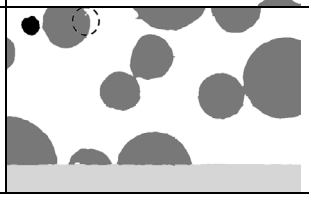	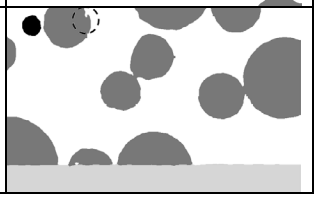

[20], as well as selecting training parameters for more accurate network operation, and many of them are selected only experimentally [21]. Thus, training a neural network and reducing the segmentation error of carbides takes a long time. However, in the future, the network will determine the volume fraction of carbides in images in the split seconds. The calculation, using the manual method according to ASTM, takes less time than training the neural network, but much more than the calculation by the network after training, and there are no prerequisites for reducing the time of this operation. Moreover, the "step" for determining the volume fraction according to ASTM, in the case of a 100-points grid, is 0.5 %, and in the case of high-quality neural network training, the accuracy will be higher. In the case of using neural networks, the statistical error in determining the average carbide content over the entire coverage area can also be reduced, since fast calculation allows increasing the number of analysed fields of vision.

The networks trained in this work are characterised by good pore recognition, and excellent segmentation of spherical

Table 2. *The fraction of carbides in the microstructure of coatings determined by different methods, %*
Таблица 2. *Доля карбидов в микроструктуре покрытий, определенная различными методами, %*

No. of image	Manual marking	Calculation according to ASTM	Network with IoU Loss	Network with Dice Loss
1	15.8	16.5	15.7	15.6
2	48.4	49.0	48.5	48.5
3	36.6	35.5	37.7	37.2
4	28.5	28.0	27.9	28.3
5	36.2	37.5	36.6	36.7

Table 3. *Mean square error, IoU, Dice, and MeanIoU metrics for different methods of determining the fraction of carbides*
Таблица 3. *Среднеквадратическая ошибка, метрики IoU, Dice и MeanIoU для разных методов определения доли карбидов*

Methods of determining the fraction of carbides	Mean square error	IoU	Dice	MeanIoU
Calculation according to ASTM	0.80	–	–	–
Network with IoU Loss	0.37	0.958	0.979	0.952
Network with Dice Loss	0.14	0.956	0.977	0.945

carbides, regardless of the imaging method (optical/electron microscope), and can now be successfully applied to estimate the volume fraction of spherical carbides in the microstructure of coatings.

There are some problems with segmentation of angular carbides, which may be related both to the lower number of images with this type of carbides in the network training set, and to the fact that such carbides were large (relative to the total image area) in the tested images and therefore not adequately estimated by networks trained on small (224×224 pixels) image fragments.

The solution to these problems can be either expanding the dataset, in particular adding images with angular carbides, and situations where the carbide takes up most of the frame, or changing the network training parameters: training on larger images, testing other loss functions, varying the size of the batch size, learning rate, etc.

CONCLUSIONS

The study shows the principal possibility of using two neural networks based on DeepLab-v3 trained with different loss functions (IoU Loss and Dice Loss) for semantic segmentation of carbides in the microstructure of composite coatings and subsequent calculation of their volume fraction. The networks recognise pores, areas not related to the microstructure and perfectly segment spherical carbides in images, regardless of their colour relative to the matrix and the presence of pores in the structure.

The values of the volume fraction of carbides determined by both networks differed from the reference values by smaller amounts than the values calculated by the manual point method according to ASTM. The network with IoU Loss is characterised by the maximum values of all IoU, Dice, and MeanIoU metrics compared to the network with Dice Loss, which indicates a smaller error in the segmentation of areas.

The main problem of the networks was the segmentation of a large angular carbide, which can be solved by expanding the dataset and changing the neural network training parameters.

REFERENCES

1. Savrai R.A., Gladkovsky S.V., Lepikhin S.V., Kolobylin Yu.M. Approaches to the development of wear-resistant laminated metal composites. *Diagnostics, Resource and Mechanics of materials and structures*, 2021, no. 5, pp. 24–35. DOI: 10.17804/2410-9908.2021.5.24-35.
2. Soboleva N.N., Nikolaeva E.P., Makarov A.V., Malygina I.Yu. The influence of chromium carbide additive on the structure and abrasive wear resistance of the NiCrBSi coating formed by laser cladding. *Vektor nauki Tolyattinskogo gosudarstvennogo universiteta*, 2020, no. 1, pp. 68–76. DOI: 10.18323/2073-5073-2020-1-68-76.
3. Pribytkov G.A., Kalita V.I., Komlev D.I. et al. Hardness and wear resistance of plasma coatings sprayed by SHS-

TiC + Ti-binder composite powders. *Uprochnyayushchie tekhnologii i pokrytiya*, 2019, vol. 15, no. 8, pp. 359–364. EDN: MROUSQ.
4. Makarov A.V., Soboleva N.N., Malygina I.Yu., Osintseva A.L. The tribological performances of a NiCrBSi – TiC laser-clad composite coating under abrasion and sliding friction. *Diagnostics, Resource and Mechanics of materials and structures*, 2015, no. 3, pp. 83–97. DOI: 10.17804/2410-9908.2015.3.083-097.
5. Nurminen J., Näkki J., Vuoristo P. Microstructure and properties of hard and wear resistant MMC coatings deposited by laser cladding. *International Journal of Refractory Metals and Hard Materials*, 2009, vol. 27, no. 2, pp. 472–478. DOI: 10.1016/j.ijrmhm.2008.10.008.
6. Enrici T.M., Dedry O., Boschini F., Tchuindjang J.T., Mertens A. Microstructural and Thermal Characterization of 316L+WC Composite Coatings obtained by Laser Cladding. *Advanced Engineering Materials*, 2020, vol. 22, no. 12, article number 2000291. DOI: 10.1002/adem.202000291.
7. Deschuyteneer D., Petit F., Gonon M., Cambier F. Processing and characterization of laser clad NiCrBSi/WC composite coatings – Influence of microstructure on hardness and wear. *Surface and Coatings Technology*, 2015, vol. 283, pp. 162–171. DOI: 10.1016/j.surfcoat.2015.10.055.
8. Zhang Z., Liu H.X., Zhang X.W., Ji S.W., Jiang Y.H. Dissolution Behavior of WC Reinforced Particles on Carbon Steel Surface during Laser Cladding Process. *Advanced Materials Research*, 2012, vol. 430-432, pp. 137–141. DOI: 10.4028/www.scientific.net/AMR.430-432.137.
9. Xu H., Huang H. Plasma remelting and injection method for fabricating metal matrix composite coatings reinforced with tungsten carbide. *Ceramics International*, 2022, vol. 48, no. 2, pp. 2645–2659. DOI: 10.1016/j.ceramint.2021.10.048.
10. Kazakov A.A., Kiselev D. Industrial Application of Thixomet Image Analyzer for Quantitative Description of Steel and Alloy's Microstructure. *Metallography, Microstructure, and Analysis*, 2016, vol. 5, pp. 294–301. DOI: 10.1007/s13632-016-0289-6.
11. Schneider C.A., Rasband W.S., Eliceiri K.W. NIH Image to ImageJ: 25 years of image analysis. *Nature Methods*, 2012, vol. 9, pp. 671–675. DOI: 10.1038/nmeth.2089.
12. Rose D., Forth J., Henein H., Wolfe T., Qureshi A.J. Automated semantic segmentation of NiCrBSi-WC optical microscopy images using convolutional neural networks. *Computational Materials Science*, 2022, vol. 210, article number 111391. DOI: 10.1016/j.commatsci.2022.111391.
13. Wang M., Wu F., Zhao J. A Comprehensive Research and Strategy of Transfer Learning for Image Segmentation. *Lecture Notes on Data Engineering and Communications Technologies book series*, 2021, vol. 88, pp. 1394–1406. DOI: 10.1007/978-3-030-70665-4_152.
14. Benjdira B., Bazi Y., Koubaa A., Ouni K. Unsupervised domain adaptation using generative adversarial networks for semantic segmentation of aerial images. *Remote Sensing*, 2019, vol. 11, no. 11, article number 1369. DOI: 10.3390/rs11111369.
15. Chen L.C., Papandreou G., Kokkinos I., Murphy K., Yuille A.L. DeepLab: Semantic Image Segmentation with Deep Convolutional Nets, Atrous Convolution, and Fully Connected CRFs. *IEEE Transactions on Pattern Analysis and Machine Intelligence*, 2018, vol. 40, pp. 834–848. DOI: 10.1109/TPAMI.2017.2699184.
16. Long J., Shelhamer E., Darrell T. Fully convolutional networks for semantic segmentation. *Proceedings of the IEEE Conference on Computer Vision and Pattern Recognition*, 2015, pp. 3431–3440. DOI: 10.1109/CVPR.2015.7298965.
17. Emelyanov A.V. Analysis of image semantic segmentation methods based on neural networks. *Matematicheskie metody v tekhnike i tekhnologiyakh – MMTT*, 2019, vol. 12-1, pp. 195–201. EDN: GCGRLL.
18. Chen L.C., Papandreou G., Schroff F., Adam H. Rethinking Atrous Convolution for Semantic Image Segmentation. *arXiv:1706.05587*, 2017. DOI: 10.48550/arXiv.1706.05587.
19. Xu H., He H., Zhang Y., Ma L., Li J. A comparative study of loss functions for road segmentation in remotely sensed road datasets. *International Journal of Applied Earth Observations and Geoinformation*, 2023, vol. 116, article number 103159. DOI: 10.1016/j.jag.2022.103159.
20. Rastorguev D.A., Sevastyanov A.A. Development of turning process digital twin based on machine learning. *Vektor nauki Tolyattinskogo gosudarstvennogo universiteta*, 2021, no. 1, pp. 32–41. DOI: 10.18323/2073-5073-2021-1-32-41.
21. Vik K.V., Druki A.A., Grigorev D.S., Spitsyn V.G. Application of deep learning neural networks for solving the problem of forest fire segmentation on satellite images. *Vestnik Tomskogo gosudarstvennogo universiteta. Upravlenie, vychislitelnaya tekhnika i informatika*, 2021, no. 55, pp. 18–25. DOI: 10.17223/19988605/55/3.

СПИСОК ЛИТЕРАТУРЫ

1. Savrai R.A., Gladkovsky S.V., Lepikhin S.V., Kolobylin Yu.M. Approaches to the development of wear-resistant laminated metal composites // Diagnostics, Resource and Mechanics of materials and structures. 2021. № 5. P. 24–35. DOI: 10.17804/2410-9908.2021.5.24-35.
2. Соболева Н.Н., Николаева Е.П., Макаров А.В., Малыгина И.Ю. Влияние добавки карбида хрома на структуру и абразивную износостойкость NiCrBSi покрытия, сформированного лазерной наплавкой // Вектор науки Тольяттинского государственного университета. 2020. № 1. С. 68–76. DOI: 10.18323/2073-5073-2020-1-68-76.
3. Прибытков Г.А., Калита В.И., Комлев Д.И. и др. Твердость и износостойкость плазменных покрытий, напыленных СВС-композиционными порошками TiC + Ti-связка // Упрочняющие технологии и покрытия. 2019. Т. 15. № 8. С. 359–364. EDN: MROUSQ.
4. Makarov A.V., Soboleva N.N., Malygina I.Yu., Osintseva A.L. The tribological performances of a NiCrBSi – TiC laser-clad composite coating under abrasion and sliding friction // Diagnostics, Resource and Mechanics of materials and structures. 2015. № 3. P. 83–97. DOI: 10.17804/2410-9908.2015.3.083-097.

5. Nurminen J., Näkki J., Vuoristo P. Microstructure and properties of hard and wear resistant MMC coatings deposited by laser cladding // International Journal of Refractory Metals and Hard Materials. 2009. Vol. 27. № 2. P. 472–478. DOI: 10.1016/j.ijrmhm.2008.10.008.
6. Enrici T.M., Dedry O., Boschini F., Tchuindjang J.T., Mertens A. Microstructural and Thermal Characterization of 316L+WC Composite Coatings obtained by Laser Cladding // Advanced Engineering Materials. 2020. Vol. 22. № 12. Article number 2000291. DOI: 10.1002/adem.202000291.
7. Deschuyteneer D., Petit F., Gonon M., Cambier F. Processing and characterization of laser clad NiCrBSi/WC composite coatings – Influence of microstructure on hardness and wear // Surface and Coatings Technology. 2015. Vol. 283. P. 162–171. DOI: 10.1016/j.surfcoat.2015.10.055.
8. Zhang Z., Liu H.X., Zhang X.W., Ji S.W., Jiang Y.H. Dissolution Behavior of WC Reinforced Particles on Carbon Steel Surface during Laser Cladding Process // Advanced Materials Research. 2012. Vol. 430-432. P. 137–141. DOI: 10.4028/www.scientific.net/AMR.430-432.137.
9. Xu H., Huang H. Plasma remelting and injection method for fabricating metal matrix composite coatings reinforced with tungsten carbide // Ceramics International. 2022. Vol. 48. № 2. P. 2645–2659. DOI: 10.1016/j.ceramint.2021.10.048.
10. Kazakov A.A., Kiselev D. Industrial Application of Thixomet Image Analyzer for Quantitative Description of Steel and Alloy's Microstructure // Metallography, Microstructure, and Analysis. 2016. Vol. 5. P. 294–301. DOI: 10.1007/s13632-016-0289-6.
11. Schneider C.A., Rasband W.S., Eliceiri K.W. NIH Image to ImageJ: 25 years of image analysis // Nature Methods. 2012. Vol. 9. P. 671–675. DOI: 10.1038/nmeth.2089.
12. Rose D., Forth J., Henein H., Wolfe T., Qureshi A.J. Automated semantic segmentation of NiCrBSi-WC optical microscopy images using convolutional neural networks // Computational Materials Science. 2022. Vol. 210. Article number 111391. DOI: 10.1016/j.commatsci.2022.111391.
13. Wang M., Wu F., Zhao J. A Comprehensive Research and Strategy of Transfer Learning for Image Segmentation // Lecture Notes on Data Engineering and Communications Technologies book series. 2021. Vol. 88. P. 1394–1406. DOI: 10.1007/978-3-030-70665-4_152.
14. Benjdira B., Bazi Y., Koubaa A., Ouni K. Unsupervised domain adaptation using generative adversarial networks for semantic segmentation of aerial images // Remote Sensing. 2019. Vol. 11. № 11. Article number 1369. DOI: 10.3390/rs11111369.
15. Chen L.C., Papandreou G., Kokkinos I., Murphy K., Yuille A.L. DeepLab: Semantic Image Segmentation with Deep Convolutional Nets, Atrous Convolution, and Fully Connected CRFs // IEEE Transactions on Pattern Analysis and Machine Intelligence. 2018. Vol. 40. P. 834–848. DOI: 10.1109/TPAMI.2017.2699184.
16. Long J., Shelhamer E., Darrell T. Fully convolutional networks for semantic segmentation // Proceedings of the IEEE Conference on Computer Vision and Pattern Recognition. 2015. P. 3431–3440. DOI: 10.1109/CVPR.2015.7298965.
17. Емельянов А.В. Анализ методов семантической сегментации изображений на основе нейронных сетей // Математические методы в технике и технологиях – ММТТ. 2019. Т. 12-1. С. 195–201. EDN: GCGRLL.
18. Chen L.C., Papandreou G., Schroff F., Adam H. Rethinking Atrous Convolution for Semantic Image Segmentation // arXiv:1706.05587. 2017. DOI: 10.48550/arXiv.1706.05587.
19. Xu H., He H., Zhang Y., Ma L., Li J. A comparative study of loss functions for road segmentation in remotely sensed road datasets // International Journal of Applied Earth Observations and Geoinformation. 2023. Vol. 116. Article number 103159. DOI: 10.1016/j.jag.2022.103159.
20. Расторгуев Д.А., Севастьянов А.А. Разработка цифрового двойника процесса точения на основе машинного обучения // Вектор науки Тольяттинского государственного университета. 2021. № 1. С. 32–41. DOI: 10.18323/2073-5073-2021-1-32-41.
21. Вик К.В., Друки А.А., Григорьев Д.С., Спицын В.Г. Применение нейронных сетей глубокого обучения для решения задачи сегментации лесных пожаров на спутниковых снимках // Вестник Томского государственного университета. Управление, вычислительная техника и информатика. 2021. № 55. С. 18–25. DOI: 10.17223/19988605/55/3.

Определение объемной доли первичных карбидов в микроструктуре композиционных покрытий с применением семантической сегментации

Соболева Наталья Николаевна*[1,2,3], кандидат технических наук, старший научный сотрудник
Мушников Александр Николаевич[1,4], кандидат технических наук, научный сотрудник
[1]*Институт машиноведения имени Э.С. Горкунова Уральского отделения РАН, Екатеринбург (Россия)*
[2]*Институт физики металлов имени М.Н. Михеева Уральского отделения РАН, Екатеринбург (Россия)*

***E-mail: soboleva@imach.uran.ru, natashasoboleva@list.ru**

[3]ORCID: https://orcid.org/0000-0002-7598-2980
[4]ORCID: https://orcid.org/0000-0001-7073-6476

Поступила в редакцию 14.06.2023 *Принята к публикации 15.08.2023*

Аннотация: В процессе формирования композиционных покрытий возможно частичное растворение упрочняющих частиц (чаще всего карбидов) в матрице, поэтому в ряде случаев выбор режима создания материала осуществляется с учетом объемной доли первичных, не растворившихся при нанесении покрытий карбидов. Широко используемые в настоящее время методы расчета объемной доли карбидов в структуре композиционных покрытий (ручной точечный метод и программы, реализующие классические методы машинного зрения) имеют ограничения по возможности автоматизации. Ожидается, что выполнение семантической сегментации с использованием сверточных нейронных сетей повысит как производительность процесса, так и точность определения карбидов. В работе проводилась многоклассовая семантическая сегментация, включающая классификацию на изображении пор и областей, не являющихся микроструктурой. Использовались две нейронные сети на основе DeepLab-v3, обученные с разными функциями потерь (IoU Loss и Dice Loss). Исходными данными были изображения различных размеров с электронного и оптического микроскопов, с карбидами сферической и угловатой формы темнее и светлее матрицы, в ряде случаев – с порами и областями, не относящимися к микроструктуре. В работе представлены изображения-маски, состоящие из четырех классов, созданные вручную и двумя обученными нейронными сетями. Показано, что сети распознают поры, области, не относящиеся к микроструктуре, и отлично сегментируют на изображениях карбиды сферической формы, независимо от их цвета относительно матрицы и наличия пор в структуре. Проведено сравнение доли карбидов в микроструктуре покрытий, определенной двумя нейронными сетями и ручным точечным методом.

Ключевые слова: композиционные покрытия; карбиды; оптическая микроскопия; растровая электронная микроскопия; семантическая сегментация; нейронные сети.

Благодарности: Работа выполнена в рамках государственных заданий ИМАШ УрО РАН по темам № АААА-А18-118020790147-4 и № АААА-А18-118020790148-1 и ИФМ УрО РАН по теме «Аддитивность» № 121102900049-1.

Микроскопические изображения получены с использованием оборудования ЦКП «Пластометрия» ИМАШ УрО РАН.

Статья подготовлена по материалам докладов участников XI Международной школы «Физическое материаловедение» (ШФМ-2023), Тольятти, 11–15 сентября 2023 года.

Для цитирования: Соболева Н.Н., Мушников А.Н. Определение объемной доли первичных карбидов в микроструктуре композиционных покрытий с применением семантической сегментации // Frontier Materials & Technologies. 2023. № 3. С. 95–102. DOI: 10.18323/2782-4039-2023-3-65-9.